# Design Proposal – Student Challenge ASPE 2020

**North Carolina State University**
Parker Eaton, Lauren Micklow, Abdullah Elkodsi, Tyler Young
Supervisor: Dr. Mark Pankow

## 1. Introduction

This document details a scribe tool controller that can control the vertical scribing force up to 1N and can be integrated with an XY scanning platform to produce a mechanical ruling system.

## 2. Design Overview

The solid model of the scribe tool controller is shown in Figure 1. The device uses a voice coil actuator to translate a stage in the z-direction; the motion of this stage is constrained via four guiding flexures (Figure 1, component B.) A capacitance probe is mounted to the translating stage and is positioned above the center of the measurement flexures. The two measurement flexures are placed side by side to limit rotation and a knife blade in the center of the beam clamping the flexures is used as the target face for the capacitance probe (Figure 1.3.) Images showing the assembly on the XY scanning platform are in the appendix.

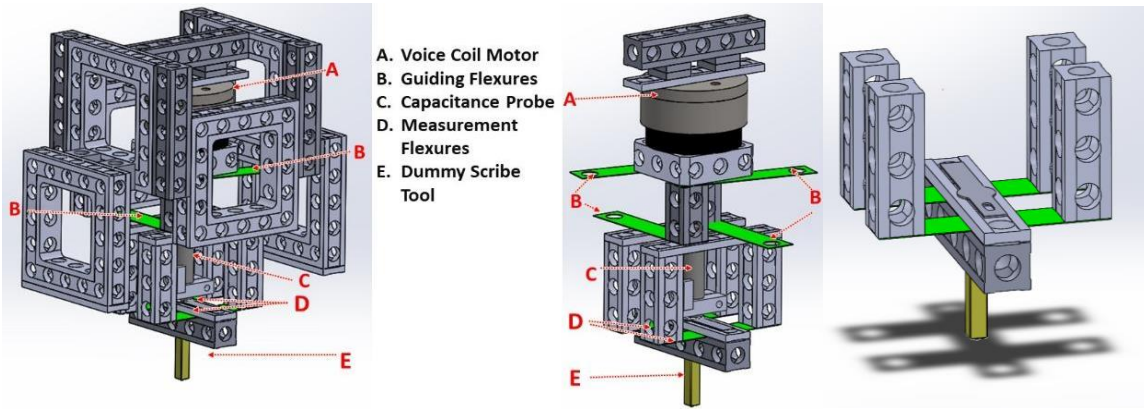


(1.1) (1.2) (1.3)

Figure 1. Full CAD model (1.1) and selective CAD models (1.2 & 1.3) to show obscured components.

The diagrams in Figure 2 show the measurement process. The voice coil applies a force to the top of the translating stage, which causes the stage to approach the part surface. As the scribe tool makes contact with the part surface, the measurement flexures bend. The capacitance sensor reads this deflection (shown in red lines in Figure 2) and, with a known flexure stiffness, the force being applied to the part may be measured.

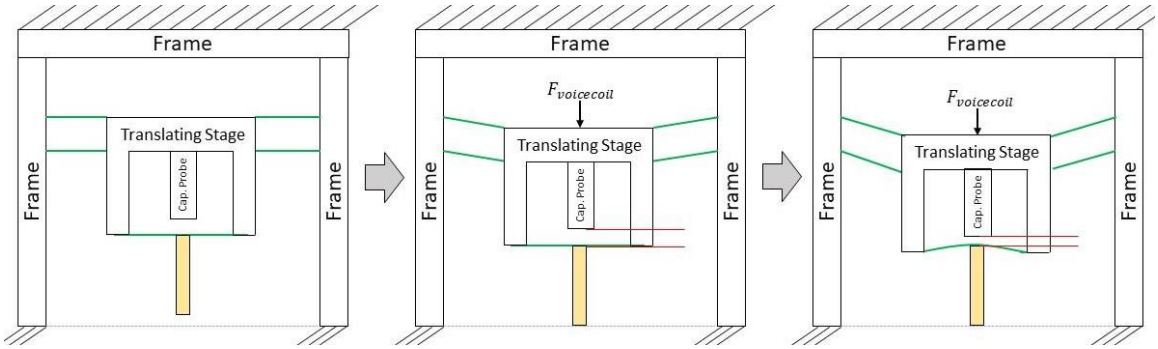


Figure 2. Diagram detailing the force measurement process

## 3. System Setup

### 3.1. Load Cell

To calibrate the load cell, five calibration masses were placed on the load platform. Based on the load cell output, a calibration scale and offset are determined and inputted into the LabVIEW controller program (Figure 3.)

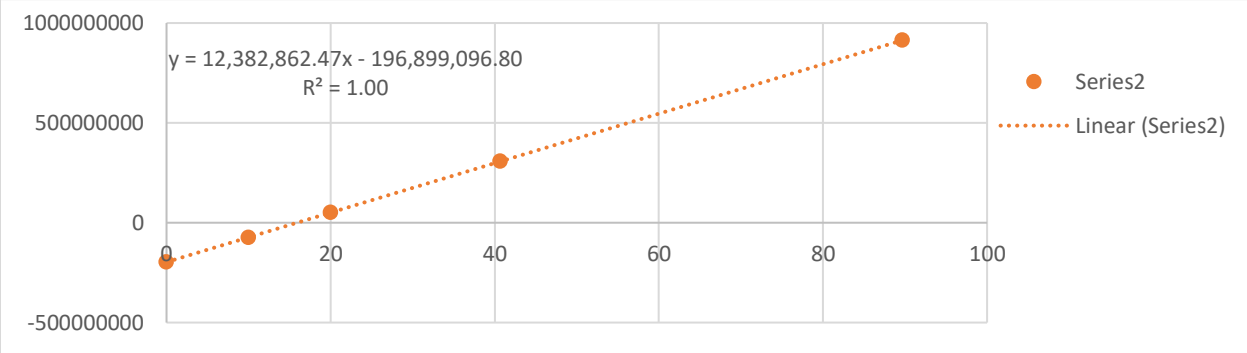


Figure 3. Load Cell Calibration

After calibration, measurements are taken to assess the performance of the load cell and the calibration. The weights were placed on the load cell, and the measurement was taken over a 10-minute period. The load cell performed the worst with the heaviest weight, with a peak percent error of 0.54% and a steady drift of +0.1g after 2 minutes. During testing, plastic deformation was observed in the loadcell despite measured loads remaining well below 100g. This necessitated frequent recalibration of the load cell and diminished the confidence held in the measurements.

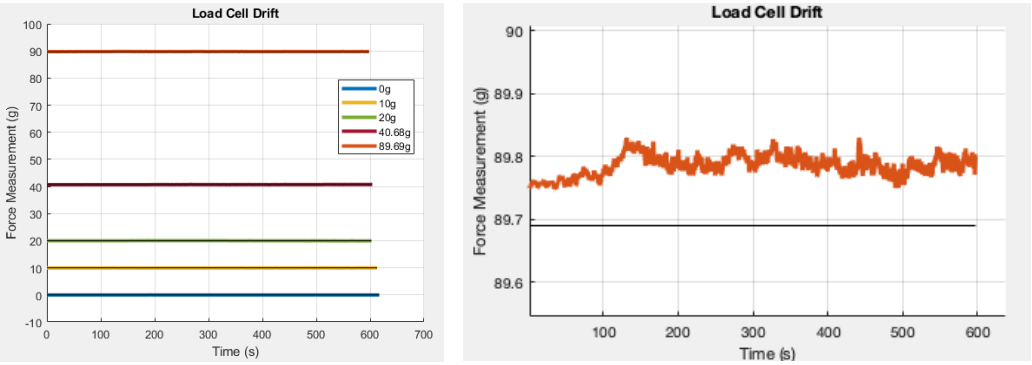


Figure 4. Load Cell Evaluation

### 3.2. Flexure Characterization

The stiffness of the flexure is estimated to be 460N/mm using data collected via LabVIEW. However, this mechanical stiffness measurement is irrelevant to the controller. To reduce errors in approximation, the flexure is modeled by a characterizing function of load cell force in terms of capacitance sensor voltage. This interpretation is an analogue of the traditional mechanical stiffness. This equation is derived from a linear fitting operation conducted with data obtained during calibration tests. Please reference section 6.1 for more information on flexure characterization.

## 4. Sensor Choice

Detecting small changes and measuring small forces in a strain gauge load cell is accomplished by quantifying very small changes in resistance. Due to the small loads, this load cell must be very soft in order to have the required resolution. A softer loadcell is a more fragile load cell, making it more susceptible to damage and necessitating frequent recalibration. The knife edge sensor has a coarse resolution and would therefore not be optimal for tracking small changes in displacement. These drawbacks motivated the decision to use only the capacitance sensor in the z-axis.

The capacitance probe has an operable range of 2mm [1]. With a flexure stiffness of 460N/mm and a deflection of 20.9$\mu$m at 1 N, it can be understood that the capacitance sensor is working well within the operable range. With a resolution of 24nm [1] and the given stiffness, the resolution is estimated to be .108g. However, the capacitance probe doesn't allow for measurement of global location when there is no force applied. To accommodate for this, during the scribing process the controller will record the voltage supplied to the voice coil at which contact is first made. An offset will be applied to account for lag and errors on the part surface.

## 5. Control Architecture and Signal Conditioning

### 5.1. Control Schematic

The governing philosophy behind the control schematic is to offer quality force control without the reliance upon a fragile, bulky, and hysteretic loadcell. This is accomplished by using a calibrated flexure for real time force measurement. Instead of controlling to a measured load from a load cell, the voltage output of a capacitance gauge is controlled. Figure 5 outlines the general approach to control. A PI controller with feedback and reinitialization was selected due to the instability observed with PID. Adding a derivative gain resulted in large and unstable oscillations in the response. From testing, it was found that a proportional gain of 1 and an integral gain of 0.03 performed very well. In block diagram form, the controller can be represented as seen in Figure 6.

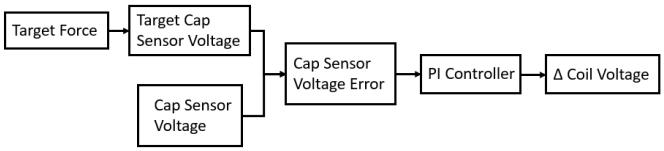


Figure 5. Control Schematic

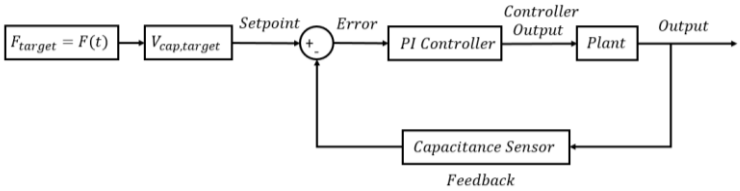


Figure 6. Block Diagram

The target force, or setpoint, is converted into a target voltage output from the capacitance sensor using a derived characterizing equation. The capacitance sensor voltage is synonymous with a target displacement of a flexure with a known stiffness. The characterizing equation is linear due to the small, linear deflections of the flexure and ease of implementation. It should be noted that an approximation of the nth order can be used if desired, though not advised due to added complexity. The error in capacitance sensor voltage is calculated by quantifying the difference between the target voltage and the measured voltage. This error is operated on by a PI controller that converts the capacitance sensor voltage error into a change in supplied voice coil voltage. Figure 7 below provides more detail regarding the calculations involved. Please note that *A* is the slope of the load cell force vs capacitance gauge voltage curve. Please find the tuned gains, characterizing equations, and information on the LabVIEW vi in the Appendix (9.3).

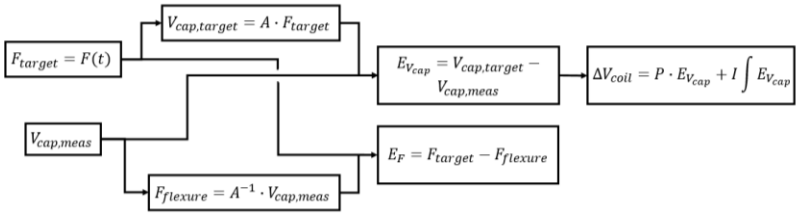


Figure 7. Detailed Control Schematic

The controller should be operated at frequencies at or below 100 Hz. An FEM was constructed in Autodesk Fusion 360 to derive the modal frequencies of the suspended mass (Appendix 9.2.) The first vibrational mode had a frequency of 163.3 Hz and a shape in the drive direction. To avoid any unwanted oscillations, the controller should be operated below this modal frequency.

# 6. Experiments

## 6.1. Calibration plots for internal force measurement

In Figure 8 below, the flexure characterization is detailed. A setpoint for the force was linearly swept from 0g to 100g while capacitance sensor voltage was recorded. The raw data was fit to a linear trend to highlight the linearity of the measured force; the measured data has an $R^2$ value of 0.038.

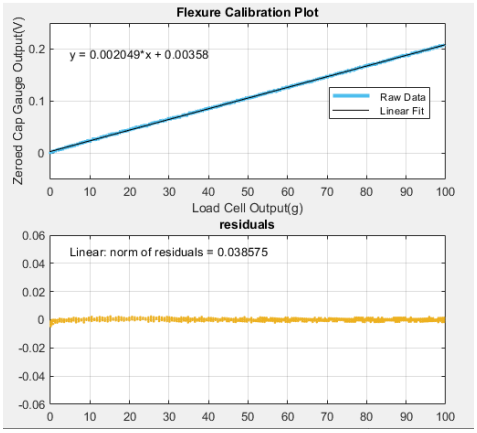


Figure 8. Flexure Calibration Curve and Residuals

The plot on the left (Figure 9) shows the error between loadcell and flexure force measurements. When the applied load was stepped, there was a sharp discrepancy between the two forces as the flexure oscillated. The load cell is less sensitive and had more lag which resulted in a smoothing of the data. Additionally, the vibration of the stage potentially impacted the flexure measurement as the capacitance sensor moves with the stage. The error between the two measurements increased with the applied load, with a maximum error of .5g. With a force of 80g, the maximum percent error is 0.63%. The stability of the measurement over time can be seen on the right. Over a period of 600 seconds, the voltage drifted by 0.005V or 0.2g. The disturbance rejection of the controller and flexure can be seen in the appendix (9.4.) The calibration of the flexure can be further tuned to decrease error in the desired force range (i.e. 40g to 100g).

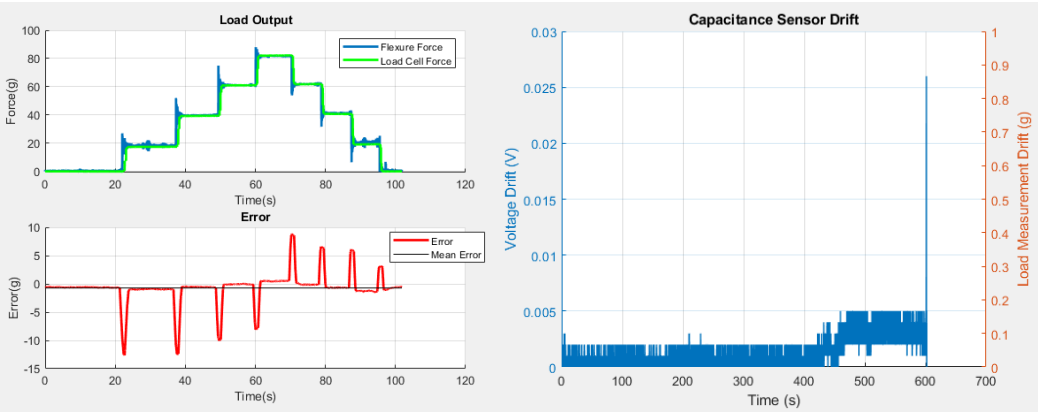


Figure 9. Flexure Response

### 6.2. Small Signal Frequency Response and Steady State Controller Error

A small signal frequency response analysis was conducted to observe how the system behaved when subjected to a range of input signals. A MATLAB code was written to generate a transfer function and a bode plot using data obtained from the trial. Figure 10 is the resulting bode plot. The data used was comprised of time, setpoint load, and measured load data arrays. Please note that the measured load array was subjected to the same hysteresis as discussed earlier, increasing the error. The system performs best at lower frequencies. This is acceptable as the controller should not encounter any high frequency inputs or disturbances while performing scribing operations.

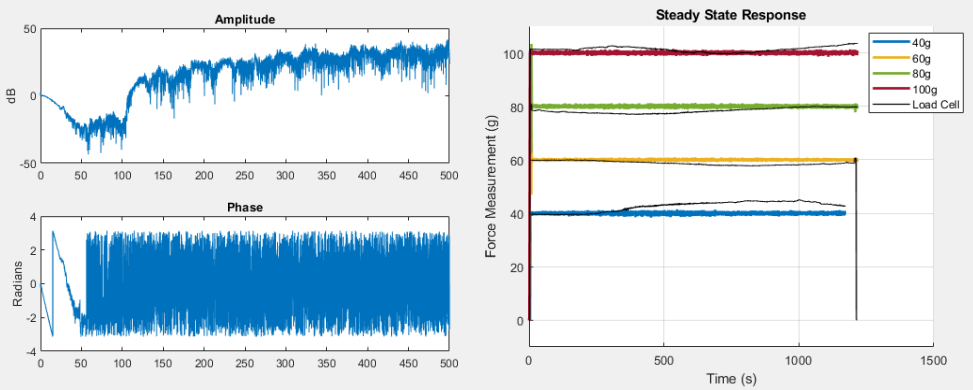


Figure 10. Small Signal Frequency Response (left) and Steady State Response (right)

Steady state controller error was evaluated for 40, 60, 80, and 100 grams over the course of 20-minute trials (Figure 10.) The force measured by the flexure was constant across each trial with minimal errors. The load cell measurement is not constant. Due to previous issues with the load cell, it is believed that this drift in measurement resulted from a problem with the load cell and not the controller as the load cell maintained this error after unloading.

### 6.3. Step Response

The step response of the system was evaluated at a range of values from 10 to 100 grams. Figure 11 shows the response at 40 and 100 grams (additional plots shown in appendix 9.5). At 40 grams, the controller reaches steady state within .3 seconds with no overshoot. At 100g the controller reached steady state within .45 seconds with an overshoot of 1.7 grams. The lag in the load cell measurement can easily be observed.

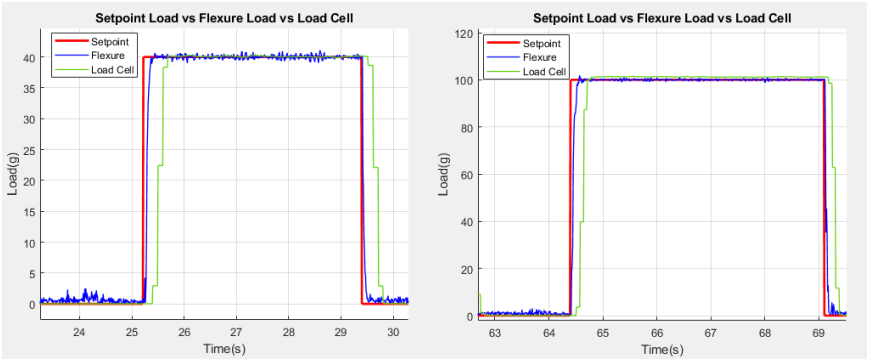


Figure 11. Step response at 40 and 100 grams

### 6.4. Ramp input

The controller generated a sine wave at .5 Hz for 30 seconds. The response is shown below (Figure 12), with the lower plot showing the load cell data shifted by -0.35 seconds to compensate for lag. When turned on, the controller was able to reach the signal at 0.6 seconds and could track the signal with a calculated phase lag of 0.05 radians. The

controller error in grams is plotted on the right vertical axis. The error never exceeds 0.05g in either direction. A detailed section of this plot is presented in the appendix (9.6).

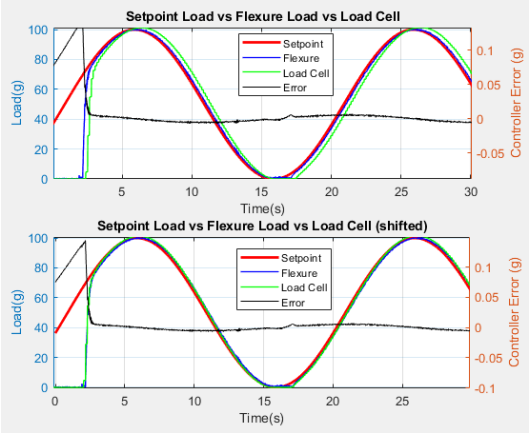


Figure 12. Ramp Input

## 7. Uncertainty Analysis

For this device there are two different sets of uncertainty that need to be considered: uncertainty stemming from the load cell itself and uncertainty from the capacitance sensor readings. The main causes for uncertainty in the capacitance gauge are shown in Table 1. The load cell uncertainty is shown in Appendix 9.7.

Table 1.Uncertainty Contributions for the Capacitance Sensor [1]

| **Uncertainty Parameter** | **Contribution** |
|---|---|
| *Linearity Error ($u_L$)* | 0.3 %F.S |
| *Error Band ($u_e$)* | 0.4 %F.S |
| *Thermal Stability ($u_t$)* | 0.04 %F.S/°C |

Thermal stability is a potential source of error, however as previously mentioned thermal effects should be minimal so long as the apparatus is kept in a controlled environment. Both the linearity error and error band provide more significant levels of error and present an adequate approximation of the uncertainty of the capacitance sensor. It was determined that the setup had slightly different contributions for this error than the device specifications. The linearity error and error band both are 0.1 % F.S higher for the setup. The total uncertainty can be calculated using the same format from the load cell calculation (Appendix 9.7) omitting temperature effects. Therefore, the capacitance sensor has a total error of 0.5 % F.S., which is a minimal difference in the quantities that it is measuring.

$$U = \sqrt{\boldsymbol{u_L^2} + \boldsymbol{u_e^2}} += \sqrt{0.3^2 + 0.4^2} = 0.5$$

## 8. Conclusion

The developed z-axis accurately responds to inputs via a LabVIEW controller via a flexure-based force measurement system. The characterized flexure allows for real time force measurement without the drawbacks of integrating a loadcell into the z-axis. A highly functional and user-friendly LabVIEW vi was developed to make operation of the force controller easy and informative. When properly calibrated and tuned, the controller quickly responds to the input with minimal error. In 2021 this z-axis will be implemented into an x-y stage, creating a mechanical ruling tool. Additional features to the controller will be added. These include a zeroing step to identify the part surface and implementing controlled motion for the x- and y-axes.

## References

[1] L. Aguirre, 2020 Student Challenge Hardware. ASPE, Aug. 2020.

# 9. Appendix

## 9.1. Frame on XY stage

Figures 14 & 15 demonstrate that the design will fit on the XY scanning platform. The top view in particular demonstrates the ability to bolt onto the existing hole pattern.

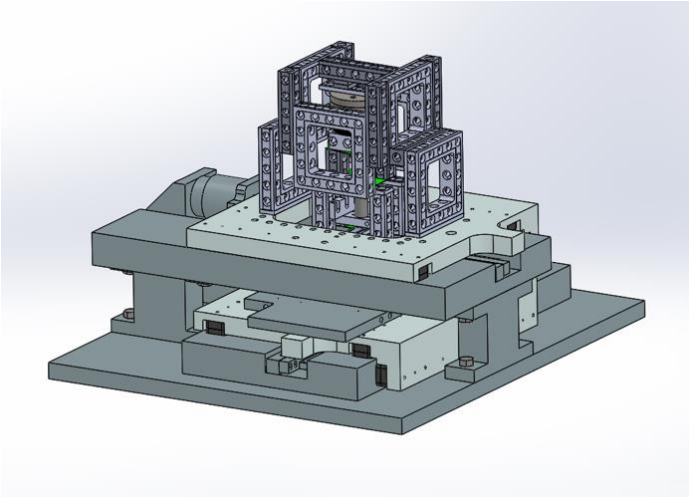

Figure 13. Isometric View

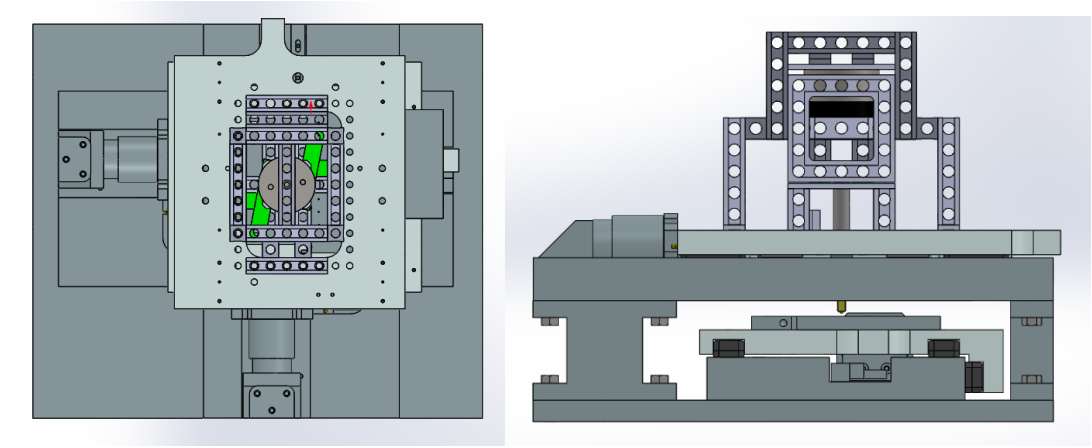

Figure 14. Top and Side Views

## 9.2. Modal Analysis

The first mode shape is shown below in Figure 15. Table 2 summarizes the results of the simulation.

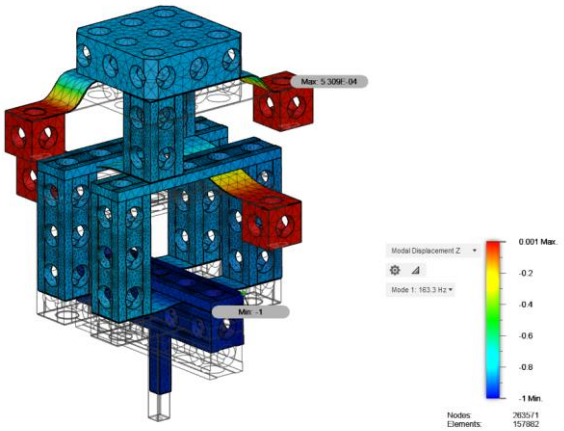


Figure 15. Vibrational Mode 1 Shape

Table 2. Modal Analysis Results

| Mode Number | Frequency (Hz) | Shape | Primary Flexure Set |
|---|---|---|---|
| 1 | 163.3 | longitudinal | Upper |
| 2 | 231.8 | Bending | Upper |
| 3 | 348.3 | Bending | Lower |
| 4 | 579.9 | Longitudinal | Lower |
| 5 | 640.7 | Bending | Lower |
| 6 | 649.4 | Bending | Upper, Middle, Lower |
| 7 | 1018 | Bending | Structural |
| 8 | 1200 | Bending | Structural |

### 9.3. LabVIEW

The PI controller and user interface were constructed in LabVIEW 2019. The vi is very capable, offering high levels of functionality with a user-friendly control panel. The user has access to three modes of operation: manual, calibration, and force control. The manual mode allows the user to change the voice coil voltage manually. Calibration offers the user the ability to run a calibration loop. The voice coil voltage is increased at a rate specified by the user until the load cell output exceeds 100g. The data from the calibration loop is used to compute the characterizing equations linking the flexure and the load cell. Lastly, the force control mode provides the user with setpoint and gain control as well as real time performance metrics. The user can select between step, sinusoidal, and ramp inputs. The proportional and integral gains can be set and updated in real time. Controller performance is tracked using the performance charts and indicators. Data is logged to a thumb drive connected to a NI myRIO and subsequently transferred to MATLAB for further analysis.

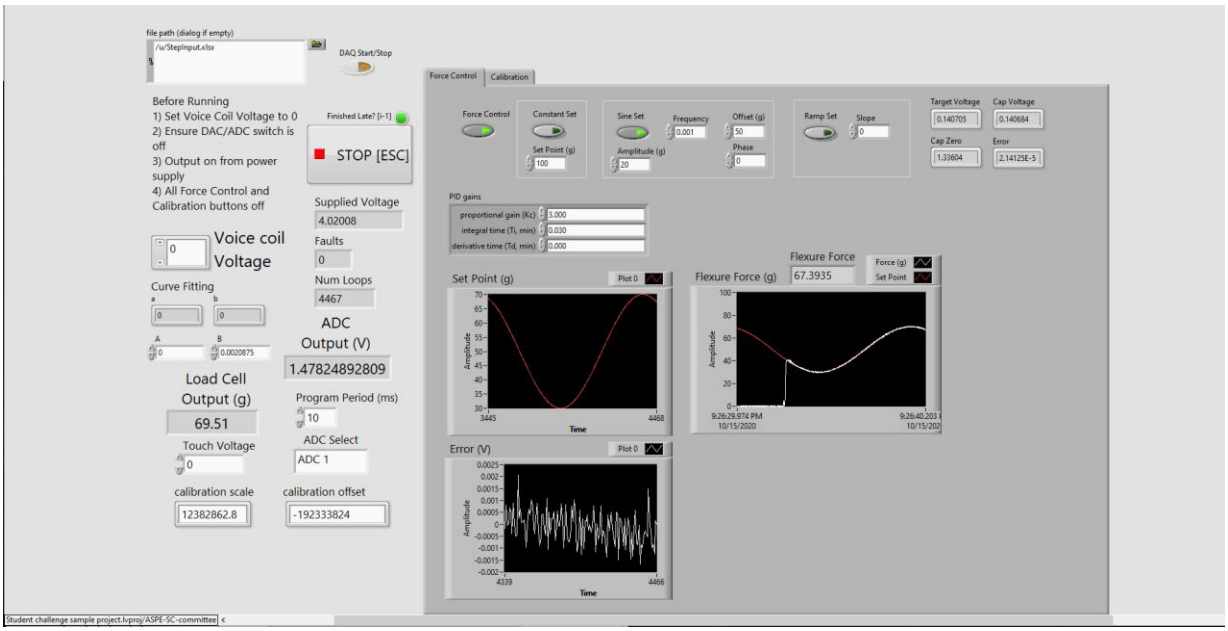


Figure 16. LabVIEW Force Control Panel

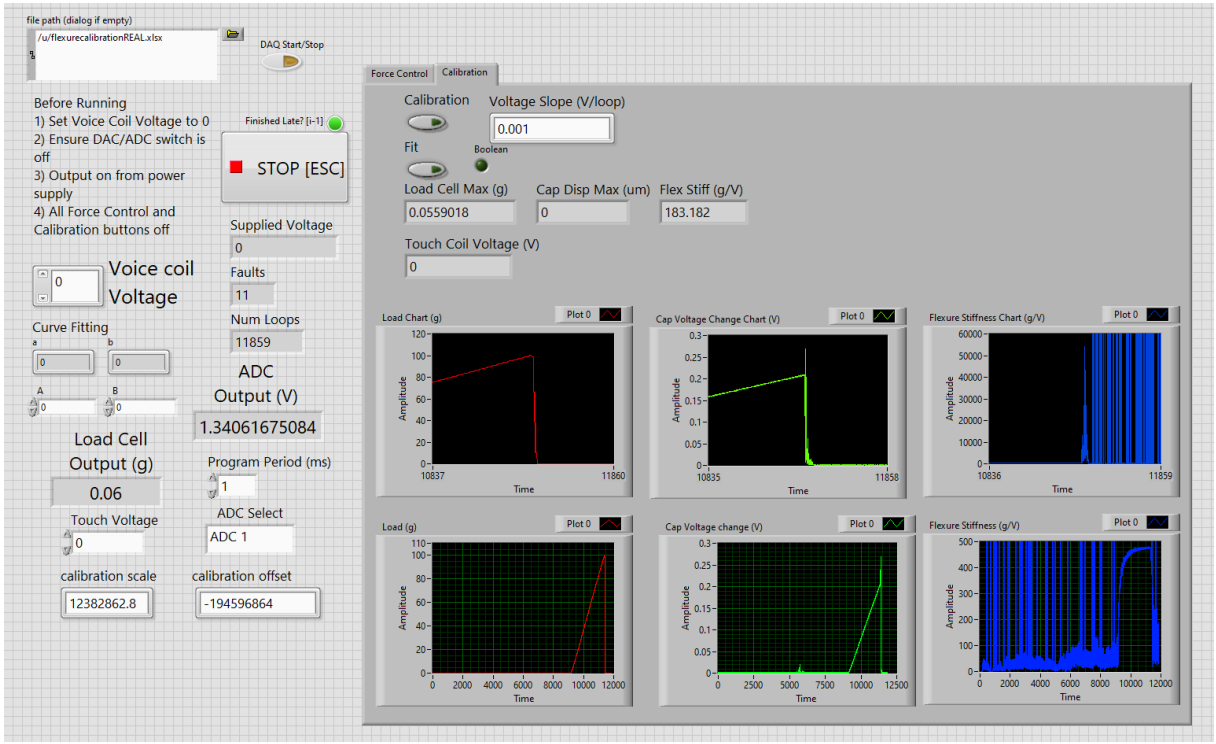


Figure 17. LabVIEW Calibration Panel

### 9.4. Disturbance Rejection

To evaluate disturbance rejection, the flexure was disturbed and the controller response was measured. Figure 18 below demonstrates the disturbance rejection of the system as well as highlights the lag and resolution of the load cell measurement compared to the flexure measurement. The load cell lags behind the flexure by 0.3 seconds and is not

able to track the high frequency disturbances. Additionally, the controller is able to reach steady state after a 70g disturbance in .6 seconds.

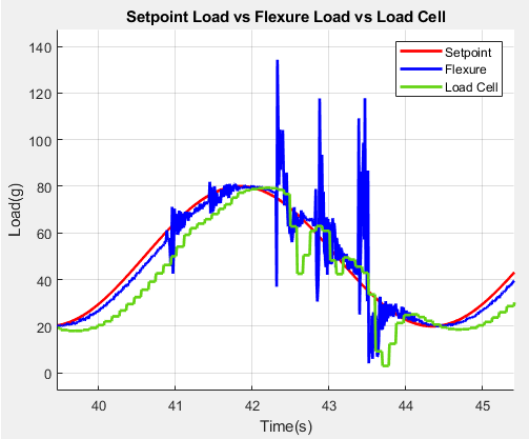


Figure 18. Disturbance Rejection

### 9.5. Step Response

Plots showing the step response at 10, 20, 30, 50, 60 & 70g. The controller had trouble with a step response at small inputs but was able to handle inputs at all other

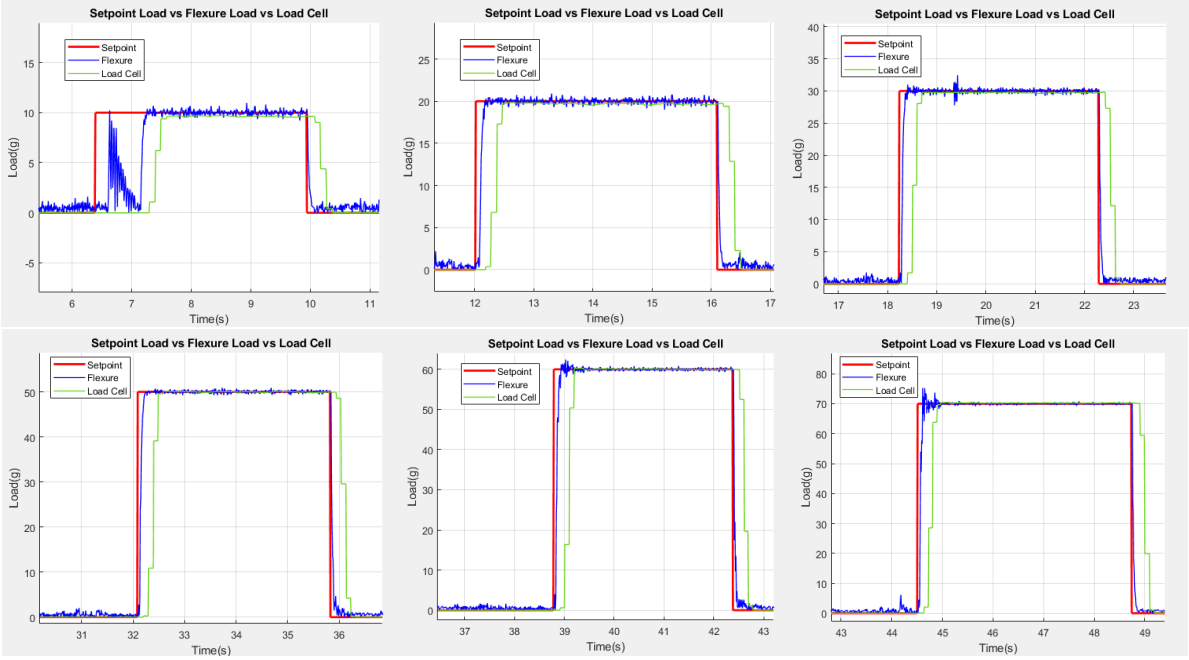


Figure 19. Additional Step Response Plots

### 9.6. Ramp Input

To better assess the controller's performance, the load cell force measurement was shifted to be in phase with the flexure force measurement. This demonstrates the capabilities of the internal force measurement technique used.

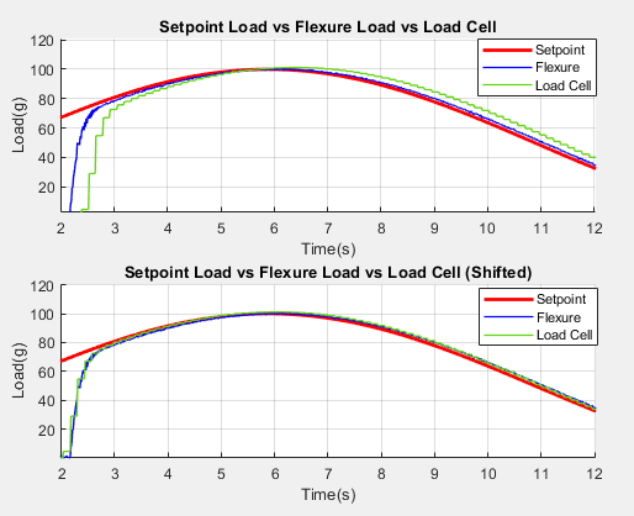


Figure 18. Influence of Load Cell Lag Compensation on Controller Performance

### 9.7. Load Cell Uncertainty

The main causes for uncertainty in the load cell are shown in Table 3.

Table 3. Uncertainty Contributions for the Load Cell [1]

| Uncertainty Parameter | Contribution |
|---|---|
| *Cell Repeatability Error Max ($u_r$)* | ± 50 mg |
| *Creep ($u_c$)* | 100 mg/hr |
| *Cell Hysteresis Max ($u_h$)* | 50 mg |
| *Temperature Effects ($u_t$)* | 5 mg/°C |

Cell repeatability error is a significant contributor to the uncertainty in the load cell and relates to the load cell's ability to maintain a constant output for a given load. This affects the load cell's weight measurement, but only up to a small percentage of its full range. Creep could prove to be a problem if the cell is run for an extended period, but in most circumstances the influence it would have on the load cell's measurements would be relatively minimal. For example, it would take half an hour for the creep to produce a level of error equivalent to the maximum possible cell repeatability error. The hysteresis of the load cell is another contributor to uncertainty; however, the impact of hysteresis decreases as the magnitude of weight change decreases. This load cell operates at a maximum load of 1 N, which is approximately 102 grams. Therefore, any weight change would be minimal, so the effect of hysteresis is not excessive. Temperature change is another factor on the measurements of a load cell, however the contribution per degree is low and temperature change should minimal so long as the apparatus remains in a controlled environment. There is residual thermal strain to consider, but it is difficult to predict the impact of thermal strain so temperature effects will be omitted from the uncertainty calculations. Total uncertainty can be obtained from the following equation.

$$U = \sqrt{\boldsymbol{u_r^2} + \boldsymbol{u_c^2} + \boldsymbol{u_h^2}} = \sqrt{50^2 + 50^2 + (100t)^2} = \sqrt{5000 + 10000t^2} = 70.7$$

When it is considered that time is in hours, and that creep has a minimal impact, the total uncertainty of the load cell becomes around 70.7 mg.